REGULAR ARTICLE

Using the Embedded Element Finite-Element Method to Simulate Impact of Dyneema® Plates

Valerie A. Martin[1] · Thomas W. Hannah[1] · Steve Ellis[2] · Reuben H. Kraft[1]

Abstract

The embedded finite-element technique provides a unique approach for modeling of fiber-reinforced composites. Meshing fibers as distinct bundles represented by truss elements embedded in a matrix material mesh allow for the assignment of more specific material properties for each component rather than homogenization of all the properties. This approach also allows for different damage and failure properties to be assigned the matrix and fiber materials which could provide new insight into the failure of the composite material, but also presents unique challenges in the implementation of the finite-element method. Here, we present a proof-of-concept model of a plate of Dyneema® under impact conditions using the embedded element method to represent the cross-ply fibers grouped into truss elements. We show that the embedded truss elements provide an easy way to implement the orthotropic material properties and transmit stress waves through the plate in a way that is consistent with images from experimental data.

Keywords Finite-element analysis (FEA) · Fibers · Polymer–matrix composites · Embedded elements

Abbreviation
UHMWPE   Ultra-high-molecular-weight polyethylene

1 Introduction

Ultra-high-molecular-weight polyethylene (UHMWPE) fiber-reinforced composites have become a popular material for ballistic armors due to their light weight and high tensile strength [1]. Dyneema® is a specific brand of UHMWPE used in armors in a 0/90 layup [2–4]. This composite usually consists of 70–85% fibers by volume held together by a polyurethane matrix. There is an ongoing effort to create an accurate and efficient finite-element model to predict the material deformation for armor design [1, 5–9]. Marco-scale models for such cross-ply composites are mostly based on a homogenization approach, where either layers of the composite or the entire composite is modeled as a homogenous continuum [3, 10–22]. While this method is computationally efficient for large-scale models, it is unable to capture the anisotropy of the alternating plies, which gives rise to the indirection tension failure mechanism [5–8], and it combines the fiber and matrix failure mechanisms making it difficult to use this type of modeling to understanding the material behavior. These mechanisms can be captured by modeling matrix and fibers discreetly [9, 23]; however, this is tedious to mesh and only reasonable to do for small-scale situations.

We propose using the embedded finite-element method to create a meso-scale model of Dyneema® that could be used to efficiently predict the material deformation and failure under impact loading. In this method, truss elements representing bundles of fibers are embedded in a matrix material by tying the displacements of the embedded truss mesh to the host element displacements. The host mesh acts as a background mesh that the truss elements can be added to arbitrarily, without any mesh continuity concerns24. This method has been used to model other composite materials, such as reinforced concrete [24–28], bio-material [29–31], and fiber-reinforced composites [32–34]. Häussler-Combe et al. have recently shown success in using the embedded element method to model cracking discontinuities in polymer reinforced composite

✉ Valerie A. Martin
  vam140@psu.edu

✉ Reuben H. Kraft
  rhk12@psu.edu

1   Department of Mechanical Engineering, The Pennsylvania State University, 320, Leonhard Building, University Park, PA 16802, USA

2   Los Alamos National Lab, P.O. Box 1663, Los Alamos, NM 87544, USA

[24]. Utomo et al. determined that using truss element to represent fibers could result in a larger stable time increment than modeling discrete layers of plies with the additional benefit of capturing fiber sliding and fracture [10].

Meshing fibers as distinct bundles represented by truss elements embedded in a matrix material mesh allows for the assignment of more specific material properties for each component rather than homogenization of all the properties. This approach also allows for different damage and failure properties to be assigned the matrix and fiber materials which could provide new insight into the failure of the composite material. By keeping the materials separate, the size of the model could be scaled from macro to micro while still using the same material properties which is useful for validating the material under different conditions [9, 35]. While homogenized material models break down at a certain length scale, using truss elements as bundles of fibers would allow a very small material sample to be modeled by simply smaller truss elements. Using a continuum material to represent the composite's matrix and embedded truss elements to represent bundles of fibers, the orthotropic nature of the material would be naturally captured. It would also be possible to map the truss elements along specific directions to model curved plates and other complex geometries which is becoming an issue in creating unique armor designs [7, 36].

In this paper, we present a proof-of-concept model of a plate of Dyneema® under impact conditions using the embedded element method to represent the cross-ply fibers grouped into truss elements. We want to show that the embedded truss elements provide an easy way to implement the orthotropic material properties and capture specific failure mechanisms observed in experimental data.

2 Methods

2.1 Plate Impact Experiments

A series of experimental tests were conducted to characterize the response of HB26 composite panels, a subset of which is used here as validation data for the model. The test being used for comparison had a single HB26 circular panel measuring one inch thick by eight inches in diameter. The plate was held in the fixture shown in Fig. 1. For this test, a single plate was clamped in rings with the bolts torqued down to 16.27 Nm (12 ft-lbs), which was selected to replicate a roughly fixed boundary condition in the clamped region, which not permanently deforming the plate due to the clamping pressure. Once clamped inside the support rings, the exposed diameter of the plate is 171.45 ± 0.762 mm (6.750 ± 0.03 in). For this test, a 9.525 mm (3/8 in)-diameter hardened tool steel ball was fired from a 0.50 caliber barrel with the use of a plastic sabot, which was captured/deflected using a series of stripper plates to minimize the potential for sabot interaction with the target panel. High-speed cameras and a chronograph were used to independently measure the velocity of the projectile, which was 1028 m/s. With this impact velocity and impact occurring at the center of the panel, the projectile was successfully captured in the target.

2.2 CT Scans and Results

After the testing was completed, the plate was scanned in a micro-CT scanner with an image resolution of 55 μm. While this is not enough to capture the roughly 17–19 um-diameter fibers, it is enough resolution to see plies, cracks, and other meso-scale features while maintaining a large field of view

Fig. 1 Experimental test fixture (left) and a close up of the clamping rings which fit into the fixture (right)
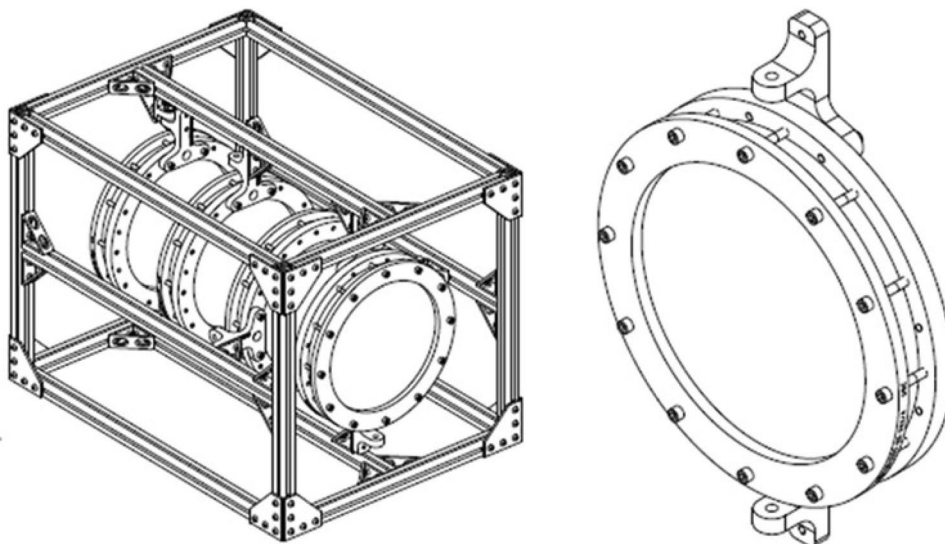
of approximately four inches by four inches and through the entire deformed thickness. A view centered on the main penetration channel is shown in Fig. 2.

Of note is the thickness of consolidated or non-delaminated composite measuring 12.85–12.90 mm representing the thickness of the shear plug or fiber cutting zone, as well as the 4.09 mm thickness of unpunctured plate remaining ahead of the projectile. Additionally, we see significant fiber/ply curling at the transition between the shear-plug dominated zone and into the delamination dominated zone. This curling is due to non-trivial deformation of the fibers when breaking, as opposed to the little to no deformation in the shear-plug failure, while the projectile velocity is still high at the beginning of the penetration event. This axial deformation or tension in the fibers causes them to retract into the plate when the fibers are broken and the energy released, creating what we call a fiber snap-back zone highlighted in Fig. 2 at the end of the shear plug failure area of the target.

2.3 Finite-Element Modeling

To model delamination as well as fiber and matrix failure, the embedded element method is combined with a layered mesh with cohesive contact between the layers. One-quarter of the 1 inch thick, 8 inch-diameter plate was modeled with 20 1.27 mm-thick layers as shown in Fig. 3a and b.

Each layer is meshed with 8880 hexahedral elements for a total of 177,600 matrix mesh elements. The mesh is seeded at 0.5 mm in the 25 mm radius near the impact zone and is allowed to be a courser seeding of 5 mm closer to the clamped edges. Each layer has 3 through thickness elements. The cohesive contact properties in Table 1 are taken from Hazzard et al. [1] Boundary conditions on the model in Fig. 3b are symmetry conditions on the two cut sides and the clamp boundary condition from the experiment is modeled by fixing all of the displacements of the front and back surfaces of the plate that would be under the clamp. The 3/8 inch spherical steel projectile is modeled as a rigid body, since no deformation was observed in the impact experiment. The full mesh of the host elements is shown in Fig. 4.

The embedded fibers were added using a custom MATLAB script. The MATLAB script takes an Abaqus input file and reads in the node connectivity of the part to host the embedded elements (Fig. 5a). The endpoints of the truss elements are determined by creating a point grid around the part and then determining which points lie within the part (Fig. 5b). The points on the edges of these bounds are specified as the endpoints (Fig. 5c) and the lines between the endpoints define the truss elements (Fig. 5d). Using this method allows the script to add truss elements to complex geometries that may include concave surfaces or internal holes. Finally, the MATLAB script

Fig. 2 X Y view (left) and X Z view (right) of the 8 inch diameter by 1 inch-thick HB26 plate when impacted by a 3/8 inch-diameter steel sphere traveling at 1028 m/s at impact
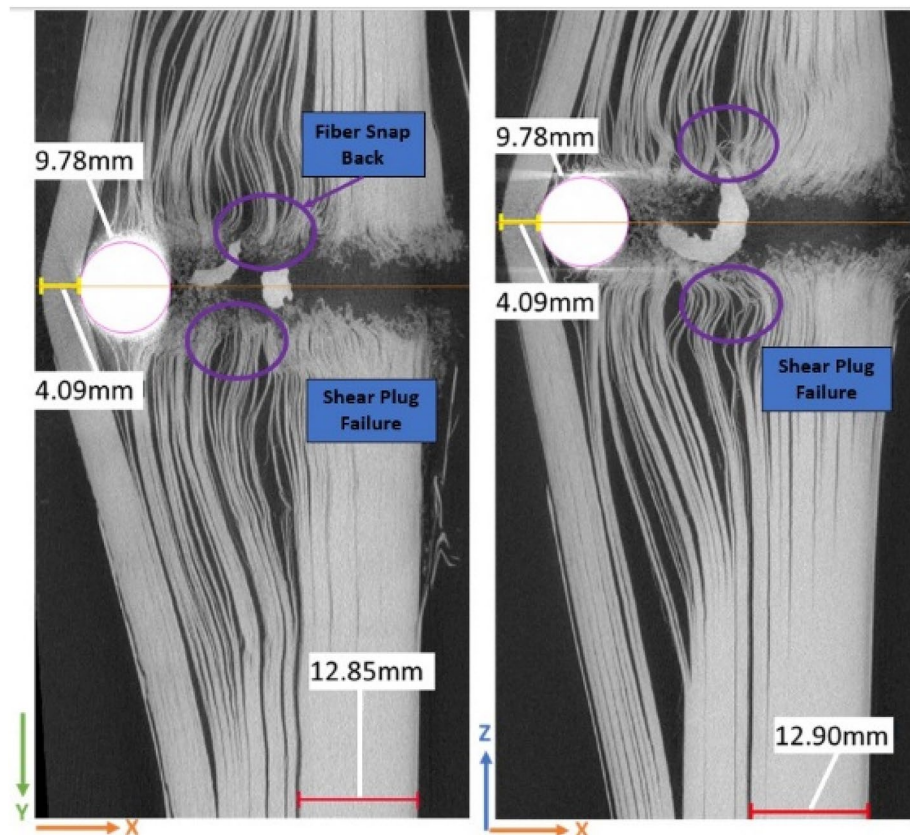
Fig. 3 **a** A single layer of matrix material, and **b** quarter symmetry finite-element model with 20 matrix layers connected by cohesive contact constraints and the clamp boundary conditions (red) and symmetry boundary conditions imposed on the model (color figure online)
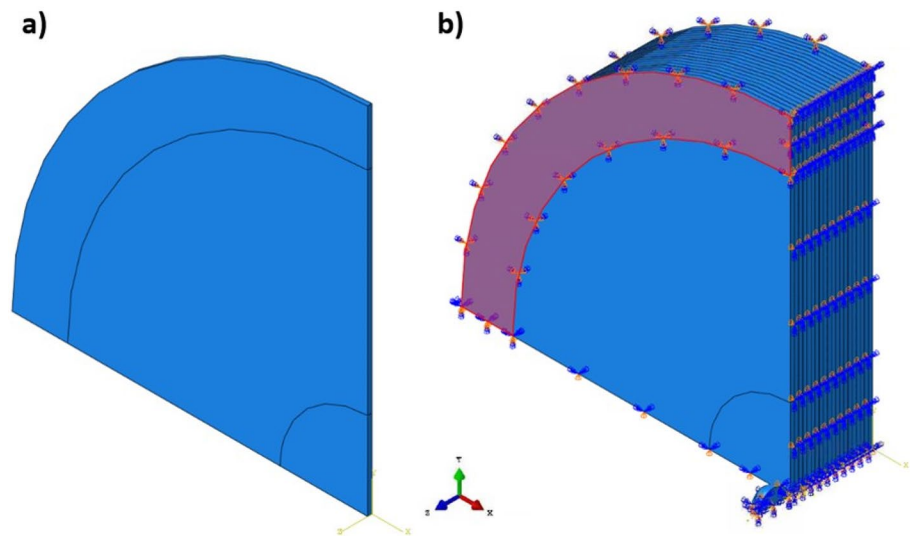
Table 1 Cohesive contact properties for the matrix layers

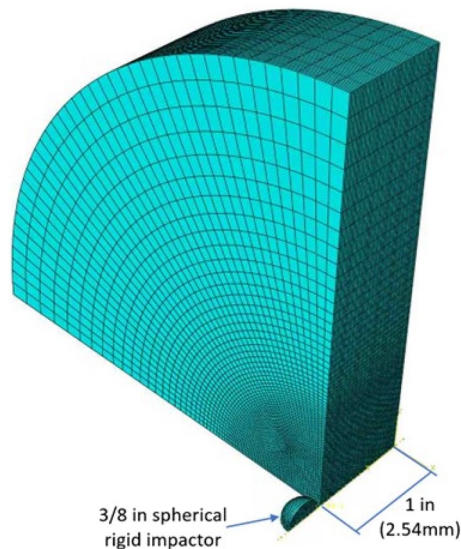|	Mode I strength	Mode I stiffness	Mode I fracture energy	Mode II strength	Mode II stiffness	Mode II fracture energy
Hazzard 2018 [1]	1.2 MPa	60 N/mm^3	0.544 N/mm	1.8 MPa	36 N/mm^3	1.088 N/mm

Fig. 4 Host element matrix mesh of 177,600 hexahedral elements

writes a new input file, complete with Abaqus's embedded element constraint that can be run by Abaqus without any further edits by the user. The number of truss elements added is determined by how many can be packed together in the part based on their cross-sectional area. The area is determined by the user by specifying the number of fibers they want each truss to represent. The area is then calculated by Eq. 1 where n is the number of fibers assigned to a truss and D_{fiber} is the fiber diameter. We assume a fiber

diameter of 17 microns (which is common for Dyneema® fibers). A larger number of fibers per truss yields less but larger truss elements for a courser mesh, while a smaller number creates a finer mesh. For this model, we tested two different fiber meshes. The first used 1380 fibers per truss (FpT) which created truss elements with a 0.632mm diameter and 405,000 total truss elements in the model. The second used 5581 FpT which created truss elements with a 1.3 mm diameter and 100,740 total truss elements. Both create a fine mesh of truss elements, as shown in Fig. 6. These two FpT numbers were chosen, because the truss diameters correspond to having two layers of 0°/90° trusses (for the 1380 FpT) or one layer of truss elements (for 5580 FpT) per 1.27 mm-thick matrix layers

$$A_{\text{truss}} = n\frac{\pi}{4}D_{\text{fiber}}^2. \tag{1}$$

Material properties for the matrix and fiber materials were chosen from literature sources and are listed in Table 2. Both components were modeled as elastic brittle, which is how the overall material as well as individually tested fibers are assumed to behave in high rate loading conditions [1, 3, 10, 37]. Material properties for just the matrix material are scarce as the overall response of the Dyneema® is assumed to be dominated by the fiber response [38, 39]. There are several studies on the high strain-rate response of fibers which suggest that they are rate dependent [37], so a rate dependency was added to the damage behavior of the fibers.
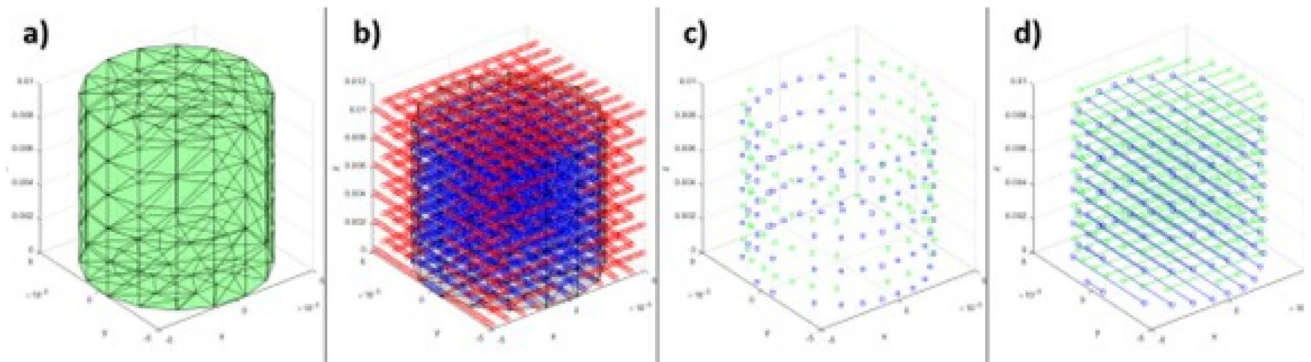
Fig. 5 Progression of creating embedded truss elements in a cylinder-shaped part

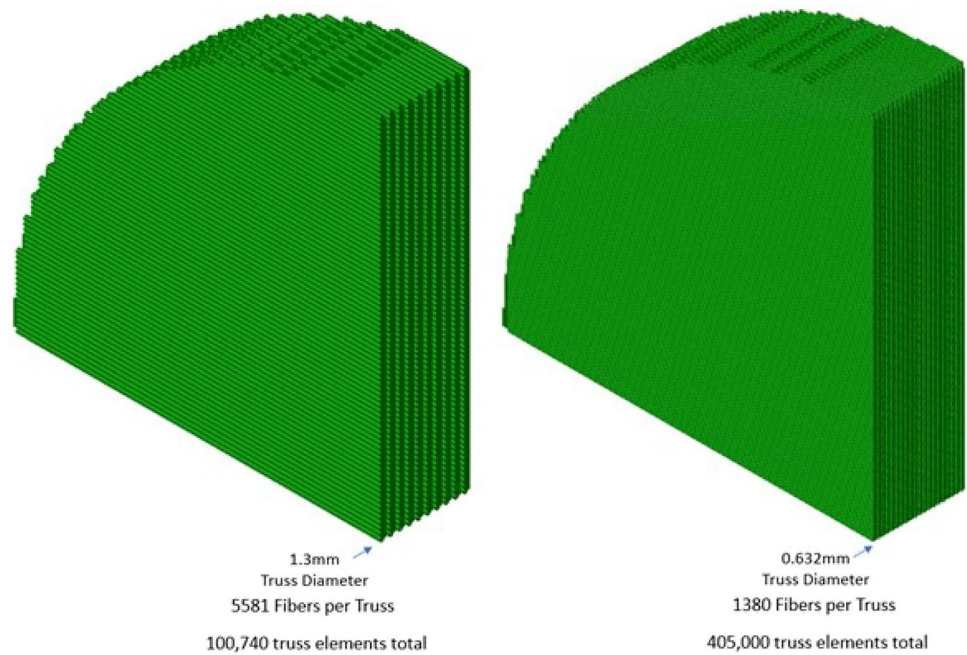**Fig. 6** Truss element meshes for the 5581 FpT and 1380 FpT meshes

1.3mm
Truss Diameter
5581 Fibers per Truss
100,740 truss elements total

0.632mm
Truss Diameter
1380 Fibers per Truss
405,000 truss elements total

Table 2 Material properties for isotropic matrix material and fibers

| Matrix material properties		Refs.	Truss material properties		Refs.
E	700 MPa	[17]	E	135 GPa	[17]
ν	0.45	[17]	ν	0.45	
ρ	980 kg/m^3	[17]	ρ	981 kg/m^3	[17]
σ_{yield}	70 MPa	[17]	$\sigma_{yield}, \dot{\epsilon}$	3.5 GPa, 0.01 1/s 4.3 GPa, 1.0 1/s 4.5 GPa, 1000 1/s	[37]
Fracture strain, $\dot{\epsilon}$	0.1, 0.01 1/s	[17]	Fracture strain, $\dot{\epsilon}$	0.0391, 0.01 1/s 0.0251, 1.0 1/s 0.01167, 1000 1/s	[37]
Fracture energy	1460 J/m^2	[51]	Fracture energy	1 J/m^2	

2.4 Modeling Challenges

We have not accounted for volume redundancy in this model, which is inherent to the embedded element method [40]. The embedded element method overlays two meshes, and since it is only mathematical, the volumes of both meshes exist in the same space. Commercial finite-element solvers do not remove any of the host element volume to account for the space occupied by embedded elements and instead leave it to the user to decide what to do about the redundancy [41]. Generally the redundancy is dealt with by reducing the stiffness and density of one or both of the mesh materials [9, 30, 42–44]. This has worked well for models with only small amounts of inclusions and quasi-static deformation but could be problematic for modeling a high fiber volume fraction material like Dyneema® in a dynamic environment where kinetic energy is non-trivial and the material sound speed matters. Since the goal of this model is to provide a proof-of-concept model to show if the embedded element method can capture some of the specific deformation mechanisms of Dyneema®, we are not addressing the volume redundancy at this time. We have other work on a way to remove the redundancy from the finite-element calculations on an algorithmic level, but that work is not advanced enough to model an impact event [40].

3 Results

Both embedded element models were run in Abaqus Explicit with parallel processing on four CPU cores. The 1380 FpT model took about 30 min to complete while the 5581 FpT model finished in under 15 min. Additionally, we tried running the 1380 FpT model using beam elements instead of the truss elements. Shear plug failure is the main failure mechanism for the first part of the impact, and we were interested in differences between using truss and beam elements, since beam elements have shear stiffness and can fail in a shear

Fig. 7 Running the embedded element model with truss elements and with beam elements produced visually similar results, with the beam elements showing more early failure and less matrix delamination than the trusses. The beam element model takes significantly longer to run
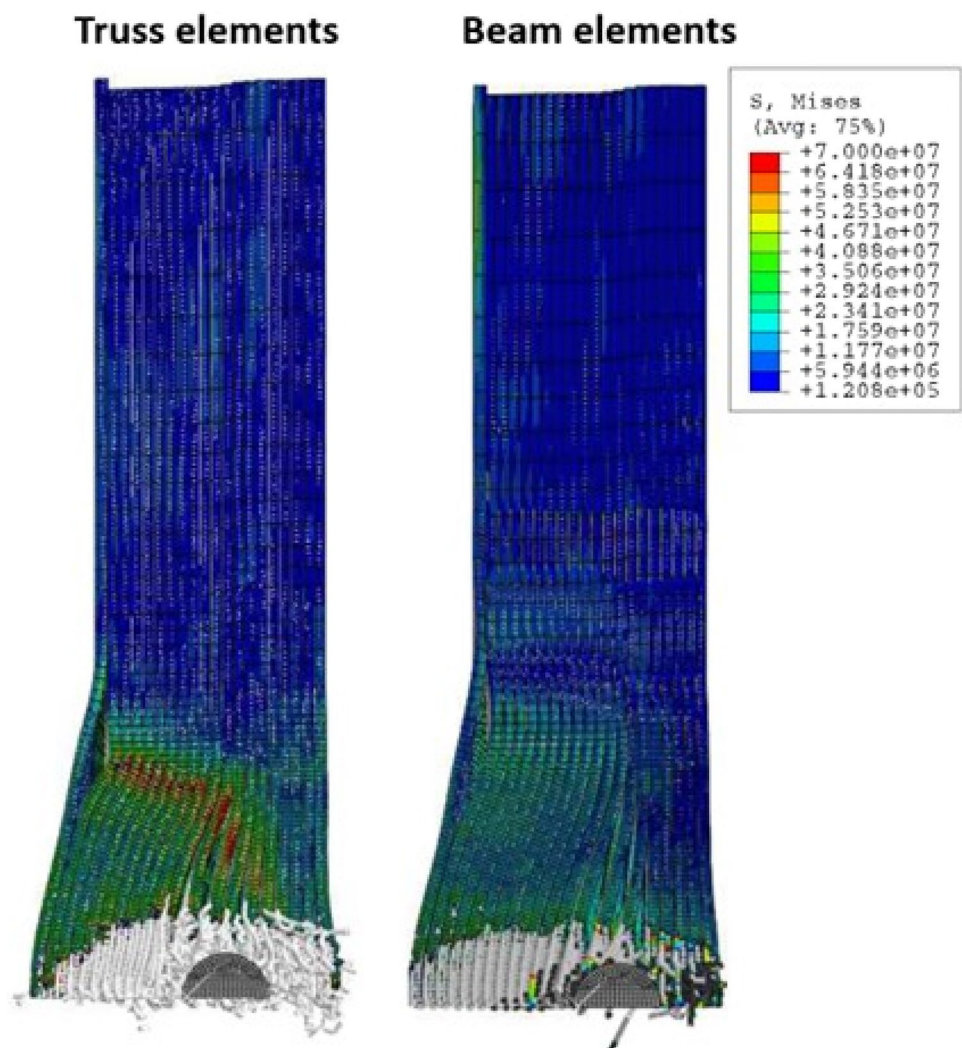
mode where trusses only support tension and compression. We found that although failure initiated sooner in the beam elements due to the addition of the shear component, the beam model took significantly longer to run than the truss model. For the same number of elements, the beam model took 12 h to run. The results between the two models in Fig. 7 look similar, so for the rest of the analysis, we chose to use the truss model.

With this embedded element model, we were looking to see if we could capture the deformation cone, shear plug failure, fiber snap back, and indication of the indirect tension mechanism. Comparison between the 1380 FpT model and the CT imaging of the plate cross section in Fig. 8 shows that, although the model projectile did not penetrate the plate as far as in the experiment, we were able to replicate some of the failure features. The initial failure zone appears to be a shear plug failure where the material plies hold together and the projectile creates a gap just wide enough for itself. The shear plug zone is also a similar size to experimental data, 10mm depth versus the experimental depth of 12.85 mm. After the shear plug failure, ply delamination becomes more dominate. With the delamination, fibers are stretched further before they fail, causing them to elastically snap back, which can be seen in both the CT imaging and in the finite-element model. A direct comparison could not be made between the back-face deformation between the model and experiment, because the penetration depth was not great enough in the model. To accommodate for this, the Von Mises stress profiles for the front and back of the plate, as demonstrated in

Fig. 9, are used to draw a comparison between the experiment and model. The characteristic deformation cone on the back face of the plate during impact is due to the stretching of the main 0 and 90° fibers across the plate. The embedded finite-element model shows this mechanism in the Von Mises stress profile on both the front and back of the plate.

The indirect tension mechanism is described as the mechanism where the transverse compressive loading of the projectile generates tension in the plies due to anisotropic expansion of the alternation 0° and 90° plies [5, 45]. Figure 10 from Liu et al. shows an illustration of the mechanism [5]. Tension in the 0° layer is transferred across the 90° layer by shear in the matrix interface between the two layers. This causes compression in the 90° layer, and then, the same matrix shear transfers this load to a tension stress in the next 0° layer.

We investigated the degree to which our embedded element model reflected this indirect tension by looking at the tensile/compression stress in the fiber layers and the shear stress in the matrix in the first microseconds of the impact, as displayed in Fig. 11. Both the 1380 FpT and 5581 FpT models showed the first 0° layer in tension, and there is a shear coupling between the first two layers of matrix material. There is significantly more shear in the 5581 FpT case, since this is the case where each matrix layer contains only a 0° or 90° layer of truss elements, while the 1380 FpT model has one of each for each matrix layer, so there is less anisotropy between layers. The compression of the second fiber layer (the 90° layer) does appear somewhat, but it is unclear if this is simply from the
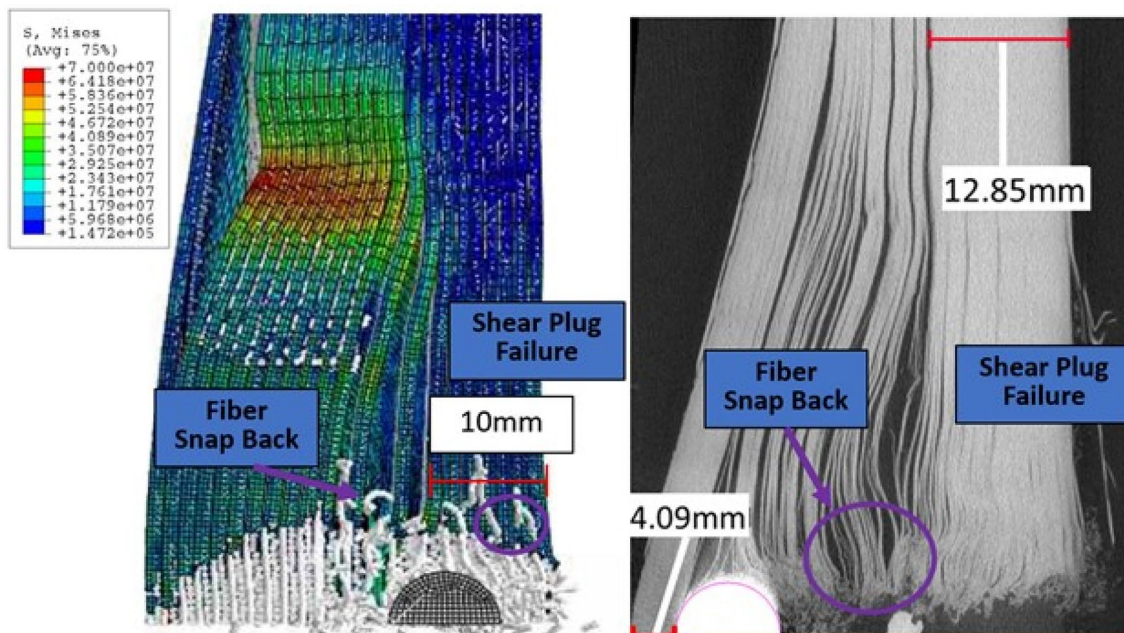

Fig. 8 When compared to CT images of the impact experiment, the embedded element model shows a similar shear plug failure zone and the fiber snap back, although the projectile penetration distance is shorter
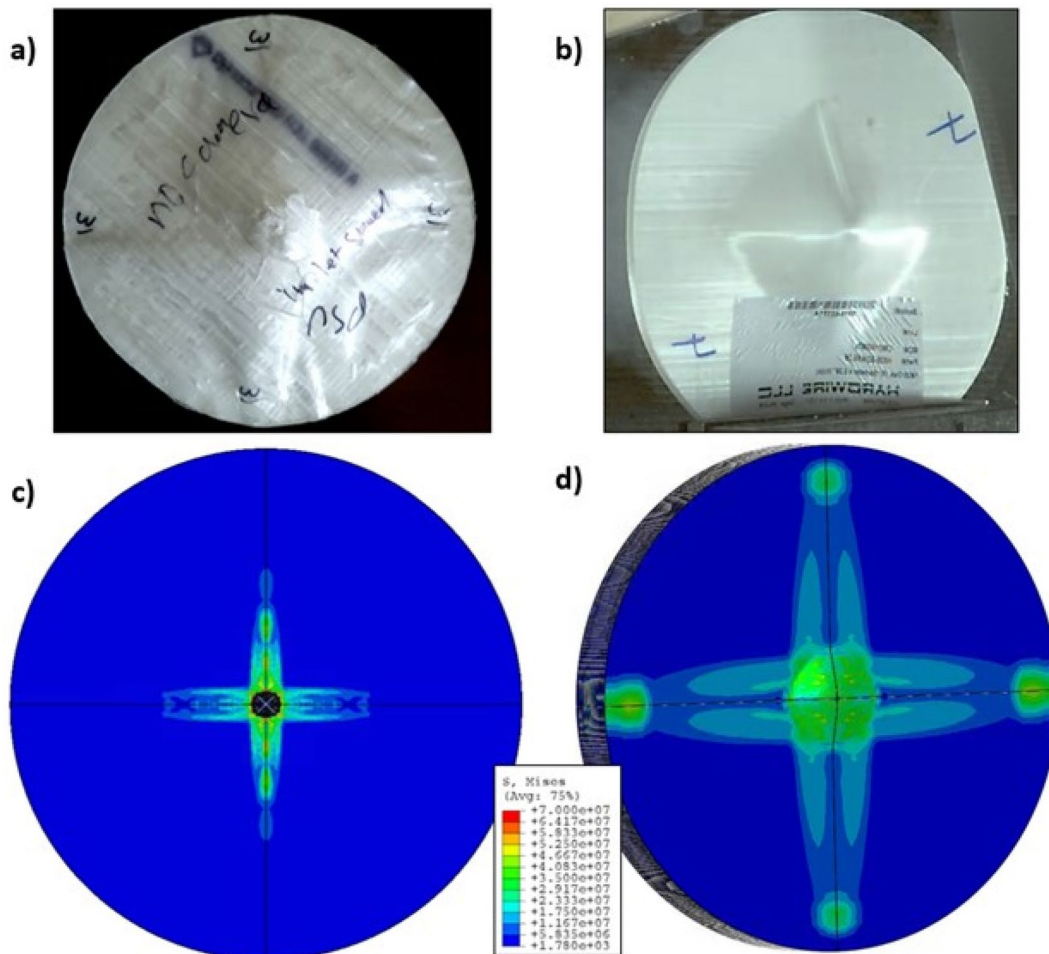
Fig. 9 **a**, **b** Examples of the deformation cone created by the stretching of the principal fibers from other impact experiments. **c** Front and **d** back-face stress patterns on the fully mirrored plate reveal the characteristic deformation cone associated with Dyneema® and other 0°/90° composites

compressive forces of the projectile or caused by the indirect tension caused by the interlaminate shear. It can be argued that this shear driven compression will not be captured by this model, since it is dependent on the change in cross-sectional area/shape of the fibers as they compress together in a group and get closer together and this model only includes one row of truss elements for each 0° and 90° layer instead of multiple as in the Fig. 10 diagram. Additionally, Abaqus does not allow for change in cross-sectional area of truss elements and assumes that they are incompressible, which will decrease the ability of the truss element layers to reproduce the compression in the 90° layer [46].

4 Discussion

4.1 Failure Mechanisms

We set out to see if modeling Dyneema® using embedded truss elements would capture some specific deformation and failure mechanisms in an impact experiment. We used cohesive contact constraints between layers of continuum element matrix material which was able to capture the delamination of Dyneema® almost exactly how it is observed in the CT images of experiments. The

Fig. 10 Sketch of the indirect tension mechanism from Liu et al. [5] with added description of the mechanisms involved

4.2 Volume Redundancy
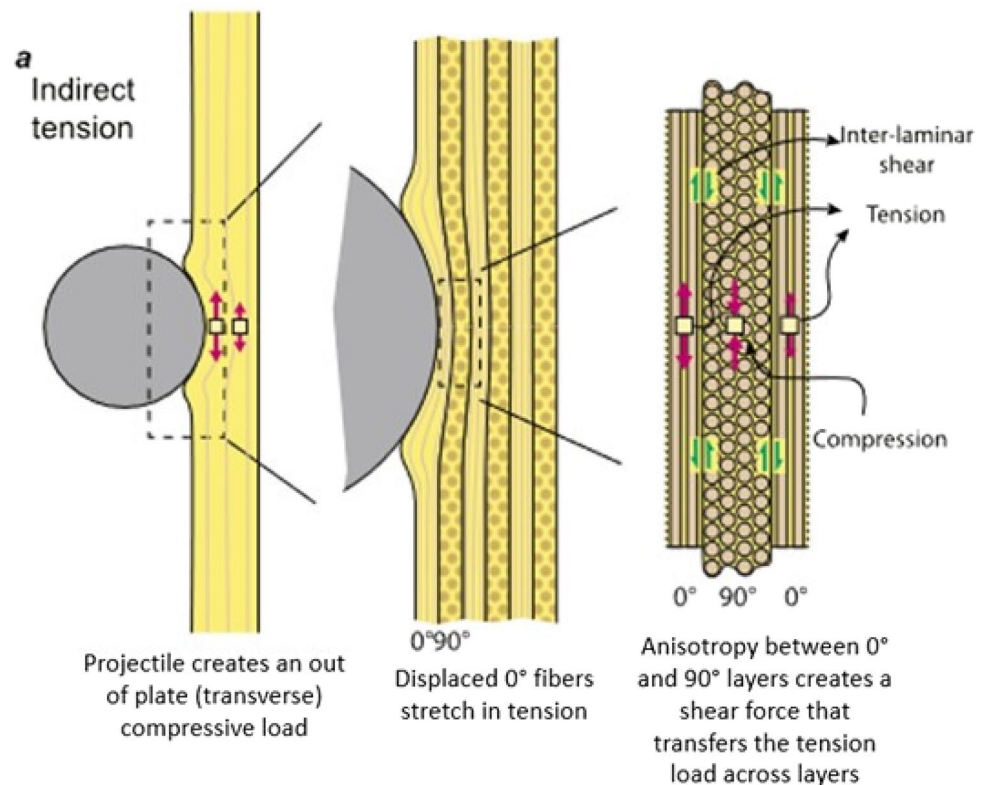
characteristic deformation cone that is formed from the stretching of the principle 0°/90° fibers during impact can also be captured by the truss elements embedded in the matrix layers. Since this is mainly seen on the back-face deformation, which the experiment used here did not experience much of, we looked at the stress profiles in the plate and were able to identify where the truss elements representing the principal fibers took most of the tensile stress. Related to this, when those principal fibers stretch and then fail, they have some elastic recovery and snap back in a distinct pattern near the beginning of the delamination regime in the penetrator's pathway. Modeling the fibers explicitly as truss elements was able to capture this feature very well. Finally, we investigated if the proposed indirect tension mechanism would appear in the model. Our model shows some features of the indirect tension mechanism, notably the shear coupling between the matrix layers. Since the truss elements only support longitudinal tensile and compression loading, they can only fail via those loadings. The fact that the embedded element model showed that an initial shear plug failure zone like the experiment means that the fibers were loaded in tension by something like the indirect tension mechanism. More work needs to be done with the arrangement of the truss elements and potentially tests using finer truss and matrix meshing to see what the size effects of the mesh are on this mechanism.

An important feature of the embedded element method that was not addressed was the volume redundancy that occurs when two meshes are superimposed on one another. This adds additional mass and stiffness to the model which impacts how the whole model behaves. Generally, redundancy is dealt with by reducing the stiffness and density of one or both mesh materials [9, 30, 42–44]. This has worked well for models with only small amounts of inclusions and quasi-static deformation but could be problematic for modeling a high fiber volume fraction material like Dyneema® in a dynamic environment where kinetic energy is non-trivial, and the material sound speed matters. We did not want to compromise those mechanics in this model, so we did not modify stiffness or density. However, we think that the extra mass and stiffness is one of the main reasons the model predicted far less penetration distance than the experiment did; there is more mass to push out of the way and the overall material is stiffer so harder to break. Future work will include comparing ways to address the redundancy and hopefully show that the redundancy needs to be dealt with on a solver level rather than just adjusting the material properties.
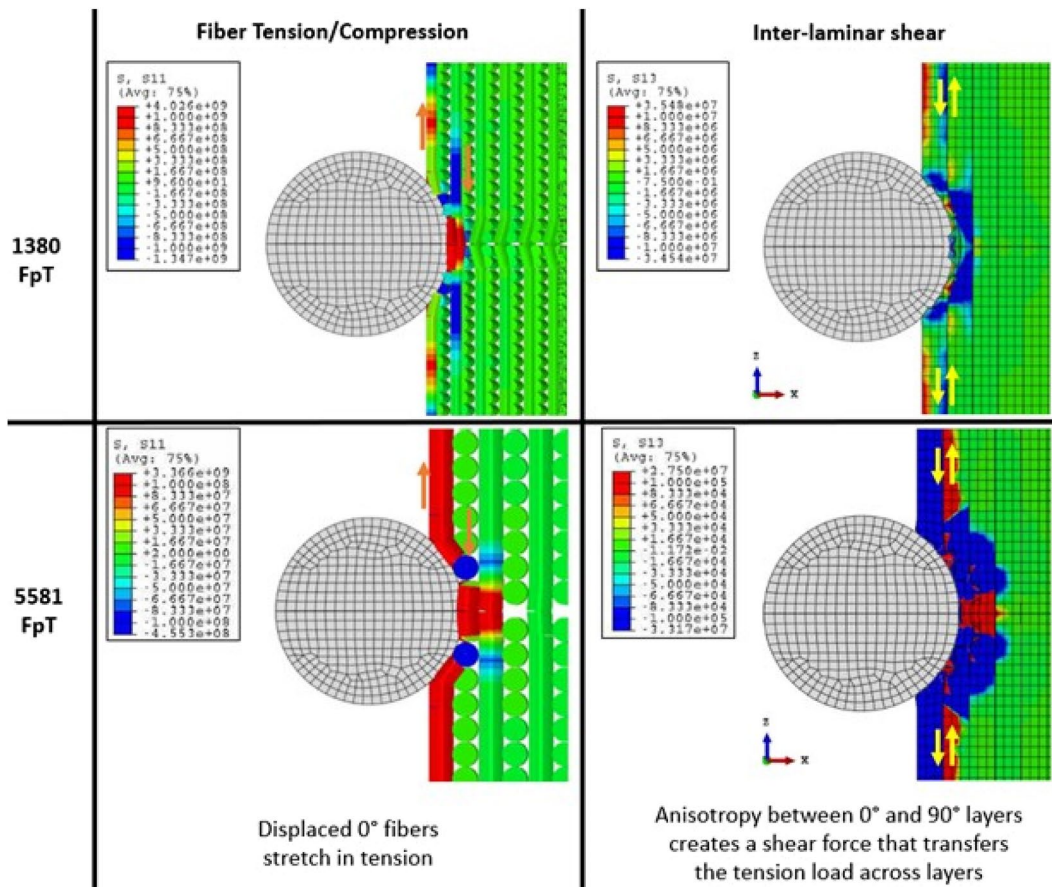
Fig. 11 Tensile/compressive stresses in the truss elements and shear stress between the matrix layers shows characteristics of the indirect tension mechanism which facilitates the tensile failure of the truss elements early in the impact process

5 Future Work

In addition to addressing the volume redundancy problem, there are a few other things that could be done to improve this model. The matrix material stiffness and failure properties could be calibrated better. There is very little research on the behavior of the matrix material, since failure is assumed to be dominated by the fibers [14, 47]. The properties used in this model have been inferred from other papers that model the entire composite by simply assuming that the matrix stiffness and failure strength is the same as the total composite in the through thickness direction. This is likely not the case and it can be seen in our embedded element model that the matrix material fails far ahead of the actual location of the projectile. Further efforts in using this type of modeling will need more information about the matrix stiffness and failure properties. Another component of the model that can be improved is the plate boundary conditions. The clamp boundary condition was applied as a fixed displacement to just the outside surfaces of the plate. This does not accurately capture the clamp boundary that is used in the experiment, since the added pressure could affect stress wave propagation. Additionally, the clamp would allow the edges of the plate to slide if the force was large enough to overcome the friction.

There are some studies on fiber material properties that show that the fibers have a different transverse stiffness than their longitudinal direction [48–50]. This could impact how the initial shear failure of the impact works, since the reduced through thickness strength could mean it is easier to fail the fibers in that direction. Truss elements could not capture this type of anisotropy, since they only support tensile and compressive stiffness. Using a beam type element would allow for a different through thickness stiffness, but as shown earlier in this work, the beam type elements are far less computationally efficient than truss elements, but if such a failure mechanism is shown to be important to the impact failure, they could be implemented.

6 Conclusion

In this work, we presented a proof-of-concept model of a plate of Dyneema® under impact conditions using the embedded element method to represent the cross-ply fibers

grouped into truss elements. Fibers bundled together to create truss elements of 0.632 mm (1380 FpT) and 1.3 mm (5581 FpT) were embedded into layers of matrix mesh bonded together by cohesive contacts. The results showed that the embedded element model was able to capture several salient features, including the initial shear plug failure zone and subsequent delamination and fiber snap back. Investigation of the fiber tensile stresses and the matrix shear stress under the projectile early in the impact shows features of the indirect tension mechanism, but it is unclear if the stresses are driven by the anisotropic expansion of the layers or other mechanisms. We have shown that, while beam elements have the potential to perform better, the truss element model captures these mechanisms with an efficient run time. Future work on this model includes addressing the volume redundancy inherent in the embedded element method as well as performing more validation tests with experimental data and different sized plates and acquiring more information about the matrix strength and failure mechanisms.

Author Contributions VM contributed to the design of the work, the acquisition, analysis, interpretation of data, the creation of finite-element models used in the work, and drafted and revised the paper. RK contributed to the conception and design of the work analysis, and draft revision. TH contributed to the experimental work, drafting, and draft revision. SE contributed to the conception and design of the work.

Availability of Data and Materials The data that support the findings of this study are available within this article and from the corresponding author upon reasonable request.

Declarations

Conflict of interest Reuben Kraft has a financial interest in BrainSim Technologies Inc., a company which could potentially benefit from the results of this research. This interest has been reviewed by Penn State University in accordance with its Individual Conflict of Interest policy for the purpose of maintaining the objectivity and integrity in research and is being managed.

References

1. M.K. Hazzard, R.S. Trask, U. Heisserer, M. Van Der Kamp, S.R. Hallett, Compos. A Appl. Sci. Manuf. **115**, 31 (2018)
2. M.J.N. Jacobs, J.L.J. Van Dingenen, J. Mater. Sci. **36**, 3137 (2001)
3. Y. Zhu, X. Zhang, B. Xue, H. Liu, Y. Wen, C. Xu, Appl. Sci. **10**, 1505 (2020)
4. D. Zhang, Y. Sun, L. Chen, S. Zhang, N. Pan, Mater. Design (1980–2015) **54**, 315 (2014)
5. B.G. Liu, H.N.G. Wadley, V.S. Deshpande, Int. J. Solids Struct. **178–179**, 180 (2019)
6. R.V. Raj, B.G. Liu, R.H.J. Peerlings, V.S. Deshpande, Mech. Mater. **164**, 104106 (2022)
7. Y. Li, H. Fan, X.-L. Gao, Compos. B Eng. **238**, 109890 (2022)
8. P. Hu, H. Yang, P. Zhang, W. Wang, J. Liu, Y. Cheng, Compos. Struct. **290**, 115499 (2022)
9. S.A. Tabatabaei, S.V. Lomov, Comput. Struct. **152**, 142 (2015)
10. H. Utomo, B. Deborah, P. R. Akkerman, B. H. Utomo, High-speed impact modelling and testing of dyneema composite Proefschrift Ter Verkrijging van de Graad van Doctor Aan de Technische Universiteit Delft, (2011)
11. G. Mo, Q. Ma, Y. Jin, W. Yan, Z. Li, and Z. Wu, Defence Technol. S2214914720303317 (2020)
12. A. Sharma, S. Daggumati, in *Innovation*, in *Materials Science and Engineering*. ed. by J. Chattopadhyay, R. Singh, O. Prakash (Springer Singapore, Singapore, 2019), pp.161–169
13. L.H. Nguyen, T.R. Lässig, S. Ryan, W. Riedel, A.P. Mouritz, A.C. Orifici, Compos. A Appl. Sci. Manuf. **84**, 224 (2016)
14. B.G. Liu, K. Kandan, H.N.G. Wadley, V.S. Deshpande, Int. J. Plast. **122**, 115 (2019)
15. S. D. Rajan, In: Lightweight Ballistic Composites (Elsevier, 2016), pp. 327–348
16. Y. Wen, C. Xu, S. Wang, R.C. Batra, J. Mech. Behav. Biomed. Mater. **45**, 11 (2015)
17. S. Chocron, A.E. Nicholls, A. Brill, A. Malka, T. Namir, D. Havazelet, H. van der Werff, U. Heisserer, J.D. Walker, Compos. Sci. Technol. **101**, 32 (2014)
18. T.A. Bogetti, M. Walter, J. Staniszewski, J. Cline, Compos. A Appl. Sci. Manuf. **98**, 105 (2017)
19. L. Iannucci, D. Pope, Express Polym Lett **5**, 262 (2011)
20. M. Grujicic, G. Arakere, T. He, W.C. Bell, B.A. Cheeseman, C.-F. Yen, B. Scott, Mater. Sci. Eng. A **498**, 231 (2008)
21. I. Lapczyk, J.A. Hurtado, Compos. A Appl. Sci. Manuf. **38**, 2333 (2007)
22. P.C. Chou, J. Carleone, C.M. Hsu, J. Compos. Mater. **6**, 80 (1972)
23. M.W. Joosten, M. Dingle, A. Mouritz, A.A. Khatibi, S. Agius, C.H. Wang, Compos. Struct. **136**, 554 (2016)
24. U. Häussler-Combe, A. Shehni, A. Chihadeh, Int. J. Solids Struct. **200–201**, 213 (2020)
25. I. Curosu, A. Omara, A.H. Ahmed, V. Mechtcherine, Materials **14**, 3631 (2021)
26. L. Vanalli, R.R. Paccola, H.B. Coda, Commun. Numer. Meth. Engng. **24**, 585 (2007)
27. A.K. Garg, A. Abolmaali, J. Transp. Eng. **135**, 121 (2009)
28. J. Kang, J.E. Bolander, Int. J. Fract. **206**, 245 (2017)
29. Y. Pan, D. Sullivan, D. I. Shreiber, and A. A. Pelegri, Front. Bio-eng. Biotechnol. **1**, 19 (2013)
30. S.A. Yousefsani, A. Shamloo, F. Farahmand, J. Mech. Behav. Biomed. Mater. **80**, 194 (2018)
31. H.T. Garimella, R.R. Menghani, J.I. Gerber, S. Sridhar, R.H. Kraft, Ann. Biomed. Eng. **47**, 1889 (2019)
32. B.N. Cox, W.C. Carter, N.A. Fleck, Acta Metall. Mater. **42**, 3463 (1994)
33. Q. Yang, B. Cox, J. Eng. Mater. Technol. **125**, 418 (2003)
34. E.V. Iarve, D.H. Mollenhauer, E.G. Zhou, T. Breitzman, T.J. Whitney, Compos. A Appl. Sci. Manuf. **40**, 1880 (2009)
35. J. Fish, Comput. Struct. **43**, 539 (1992)
36. S. West, Designing a Human-Centric Rigid Body Armor for Female Police Officers: The Implications of Fit on Performance and Gender Inclusivity, University of Arkansas (2019)
37. B. Sanborn, A.M. DiLeonardi, T. Weerasooriya, J. Dynamic Behavior Mater. **1**, 4 (2015)

38. S. Chocron, N. King, R. Bigger, J.D. Walker, U. Heisserer, H. van der Werff, J. Appl. Mech. **80**, 031806 (2013)

39. M. K. Hazzard, P. T. Curtis, L. Iannucci, S. Hallett, R. Trask, 12 (2015)

40. V.A. Martin, R.H. Kraft, T.H. Hannah, S. Ellis, Adv. Model. Simul. Eng. Sci. **9**, 12 (2022)

41. SIMULIA User Assistance 2022: Abaqus/Constraints/Embedded Elements.https://help.3ds.com/2022/english/dssimulia_established/SIMACAECSTRefMap/simacst-c-embeddedelement.htm?contextscope=all&id=52ee32705e334ec3a1b69df8ffd66d50#simacst-cembeddedelement-t-SpecifyingTheEmbeddedNodes-sma-topic5

42. W.-G. Jiang, S.R. Hallett, M.R. Wisnom, *Mechanical Response of Composites* (Springer, Netherlands, Dordrecht, 2008), pp.281–291

43. D. Ohyama, T. Kurashiki, Y. Watanabe, Y. Fujita, M. Zako, Estimation of mechanical behavior of braided composites based on mesh superposition method. In: International Conference on Composite Materials (2011). https://iccm-central.org/Proceedings/ICCM18proceedings/data/2.%20Oral%20Presentation/Aug25(Thursday)/Th45%20Micromechanics%20of%20Composites%20and%20Heterogeneous%20Materials%20Multiscale%20Modeling/Th45-6-AF1293.pdf

44. N.T. Chowdhury, M.W. Joosten, G.M.K. Pearce, Compos. Struct. **210**, 294 (2019)

45. J.P. Attwood, S.N. Khaderi, K. Karthikeyan, N.A. Fleck, M.R. O'Masta, H.N.G. Wadley, V.S. Deshpande, J. Mech. Phys. Solids **70**, 200 (2014)

46. J.P. Foreman, D. Porter, D. Pope, and F.R. Jones. Predicting the material properties of a polyurethane matrix (a composite within a composite), in *ECCM15-15th European Conference on Composite Materials*, (2012), pp. 24–28

47. J.P. Foreman, D. Porter, D. Pope, F.R. Jones, 5 (2012)

48. M. Hudspeth, X. Nie, W. Chen, Polymer **53**, 5568 (2012)

49. T. Frank, S. Sockalingam, S.L. Alexander, T. Weerasooriya, DEVCOM army research laboratory. in *Influence of Dynamic Multiaxial Transverse Loading on Ultra High Molecular Weight Polyethylene (UHMWPE) Dyneema SK76 Single Fiber Failure* (2020), p. 44

50. F. Thomas, S. Sockalingam, S. L. Alexander, and T. Weerasooriya, 44 (2020)

51. T. Lässig, L. Nguyen, M. May, W. Riedel, U. Heisserer, H. van der Werff, S. Hiermaier, Int. J. Impact Eng **75**, 110 (2015)